

Downloaded from UvA-DARE, the institutional repository of the University of Amsterdam (UvA)
<http://hdl.handle.net/11245/2.46782>

File ID uvapub:46782
Filename 214590y.pdf
Version unknown

SOURCE (OR PART OF THE FOLLOWING SOURCE):

Type article
Title O- holes associated with alkali acceptors in BaTiO₃
Author(s) T. Vanhorst, O.F. Schirmer, H. Kröse, R. Scharfschwerdt, Th.W. Kool
Faculty UvA: Universiteitsbibliotheek
Year 1996

FULL BIBLIOGRAPHIC DETAILS:

<http://hdl.handle.net/11245/1.426846>

Copyright

It is not permitted to download or to forward/distribute the text or part of it without the consent of the author(s) and/or copyright holder(s), other than for strictly personal, individual use, unless the work is under an open content licence (like Creative Commons).

O^- holes associated with alkali acceptors in $BaTiO_3$

T. Varnhorst, O. F. Schirmer, H. Kröse and R. Scharfschwerdt
Fachbereich Physik, Universität Osnabrück, D-49069 Osnabrück, Germany

Th. W. Kool

Laboratory for Physical Chemistry, University of Amsterdam, NL-1018 WV Amsterdam, Netherlands

(Received 7 July 1995)

In $BaTiO_3$ the alkali ions Na and K, replacing Ba, lead to acceptor levels about 50 meV above the valence band edge. The structure of these defects can be studied by electron spin resonance, after light induced valence-band holes have been captured at neighboring O^{2-} ions. Hyperfine interaction with Na, Ba, and Sr impurities, adjacent to the paramagnetic O^- , is identified. The holes are trapped stably below ~ 50 K. Their level position is determined by the temperature dependence of the relaxation rate of the light-induced non-equilibrium excess hole population. Photostimulated small polaron transfer between O^{2-} sites equivalent with respect to Na or K leads to a strong optical-absorption band with peak at 1.3 eV, corresponding to a stabilization energy of the bound hole polaron of about 0.65 eV. The Na^+-O^- dipoles can be reoriented under uniaxial stress at 4.2 K; a differential stress coupling coefficient of $1.23 \times 10^{-4} \text{ m}^3$ is derived. Several O^- centers associated with partly unassigned acceptors on Ti sites are identified. Their properties are compared to those of the Ba site acceptors. Vibronic g shifts are accounted for by a dynamic Jahn-Teller effect involving the twofold degenerate $O^- \pi$ orbitals.

I. INTRODUCTION

$BaTiO_3$ usually contains a sizeable concentration of extrinsic acceptors, strongly influencing the defect chemistry and the conductivity properties of the material.¹ Alkali ions, e.g., Na or K, incorporated on Ba sites, form an important subgroup among such acceptors. The structure and hole binding energies of these defects were not known so far. Here we report on the determination of these and related properties using electron spin resonance and complementary techniques. It is found that the $(Na^+)'$ and $(K^+)'$ centers, charged negatively with respect to the lattice, are transformed at low temperatures into their neutral states by capture of holes, created by optical excitation of valence-band electrons to deep levels, such as $Rh^{4+/3+}$. The holes are metastably trapped at one of the equivalent O^{2-} ions next to the alkali acceptor core. The structure of the resulting Na^+-O^- and K^+-O^- centers will be described; it will turn out that these defects are rather shallow, their levels lying about 50 meV above the valence-band edge. The centers are connected with strong, wide optical-absorption bands, caused by light-induced polaronic hole transfer between the O^- sites equivalent with respect to Na^+ or K^+ . The bands dominate the low-temperature light-induced coloration of such crystals. Alkali acceptors have been identified in all $BaTiO_3$ crystals which we have investigated so far.

Acceptor defects on Ba sites have to be contrasted to those replacing Ti, such as $(Al_{Ti}^{3+})'$.² Comparisons between the features of these two types of centers will be made throughout this paper.

A short account of the properties of the alkali centers has been given previously.³ Here we intend to present a rather complete overview. These defects turn out to be prototypes

of several related ones, which have been identified in oxide perovskites.⁴⁻⁸ They have similar ESR signatures as the alkali acceptors; in some cases definite submicroscopic models still are lacking.

The photosensitivity of the alkali acceptors is a feature shared with many transition metal dopings, which are involved in light-induced charge transfer processes in $BaTiO_3$ and which can be incorporated to stimulate the photorefractivity of the material. The present investigation is part of a project devoted to identify defects optimally sensitizing the photorefractive efficiency of $BaTiO_3$.

After presenting information on experimental details, the results of ESR, optical-absorption, and uniaxial stress investigations will be reported. From these studies the structural and energetical properties of the centers will be derived. A final section is devoted to a discussion of the identified facts within a wider context.

II. EXPERIMENTAL DETAILS

The investigated crystals were grown by Dr. H. Hesse and co-workers at the Crystal Growth Laboratory of the University of Osnabrück. Unpoled, nominally undoped specimens with the typical size $2 \times 3 \times 4 \text{ mm}^3$ were used as grown. A Bruker ER 200 D-SRC 9 GHz spectrometer served to take the ESR spectra, usually at temperatures between 10 and 100 K, i.e., in the rhombohedral phase of $BaTiO_3$. In order to measure light-induced absorption changes simultaneously with corresponding changes of the defect charges, as monitored by ESR, we have built a glassfiber based, fast multi-channel spectrometer, covering the wavelength range 300 to 1100 nm, which allows us to take 20 ms snapshots of light-induced absorption spectra covering the full wavelength

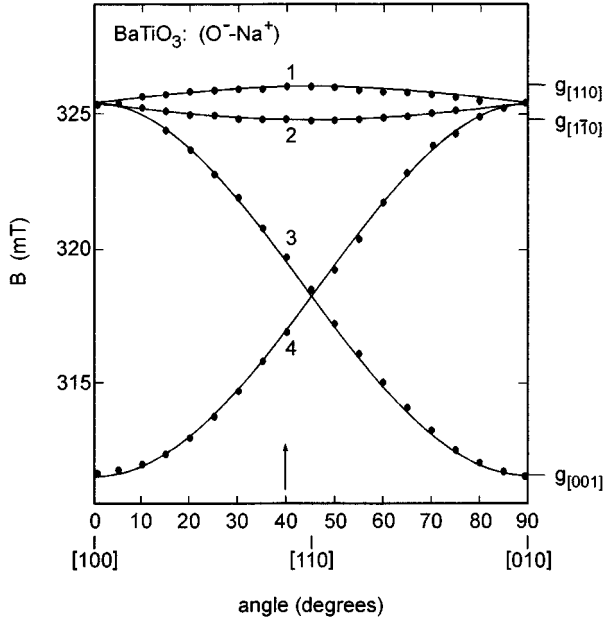


FIG. 1. Angular dependence of the resonance fields of O⁻-Na⁺ in BaTiO₃ ($\nu=9.14$ GHz, $T=10$ K). The line positions defining the principal values of the g tensor are indicated at the right side. The arrow marks the field direction at which uniaxial stress measurements (Fig. 11) have been performed.

range. The input end of the spectrometer is identical to the quartz rod holding the specimen in the center of the ESR cavity. The simultaneous measurement permits to correlate the ESR and optical phenomena in a simple way.

III. EXPERIMENTAL RESULTS AND THEIR INTERPRETATION

A. Electron spin resonance spectra

In nominally undoped BaTiO₃ crystals, ESR signals with g values in the range 1.99 to 2.11 arise after illumination at $T \leq 25$ K, their intensity depending on the photon energy in a way to be described below. The angular variation of the resonance fields of a prominent one among these centers is given in Fig. 1. It can be described by $\mathcal{H} = \mu_B \mathbf{B} \mathbf{g} \mathbf{S}$ with $S = 1/2$, the principal directions of \mathbf{g} being indicated in Fig. 1 and the principal values in Table I. These g -tensor components are typical for O⁻ trapped hole centers.⁹ Since the g values closest to g_e , the free electron g value, are expected for \mathbf{B} along the symmetry axis of an O⁻ p lobe, the model in Fig. 2 is consistent with the observed angular dependence. Further support for this model will be given below.

Higher resolution of the spectra leads to information on the surroundings of O⁻. In Fig. 3 hyperfine splitting into four intense strong lines is seen, caused by interaction with a nucleus with $I = 3/2$, 100% abundant. Among the possible choices (Be, Na, As, Tb, Au) Na is the most likely one, its presence in the (10–100) ppm range generally being proved by chemical analysis of nominally undoped BaTiO₃. Table I also contains the Na hyperfine parameters.

In Fig. 3 further hyperfine lines outside of the Na quartet are discerned. Their most likely interpretation is based on the assumption that O⁻ is surrounded additionally, as expected, by Ba²⁺ ions (¹³⁷Ba, $I = 3/2$, 11.2%, $g_n = 0.63$; ¹³⁵Ba, $I = 3/2$, 6.6%, $g_n = 0.56$).

TABLE I. Resonance parameters of the alkali-O⁻ acceptors and related defects. All hyperfine parameters in 10^{-4} cm⁻¹. x: could not be determined; *: rotation by τ around [001] direction

$\mathbf{B} \parallel$	[001]	[1 $\bar{1}$ 0]	[110]
Na ⁺ -O ⁻			
g	2.0962(3)	2.0077(3)	1.9998(3)
$ A(^{23}\text{Na}) $	1.203(5)	1.284(5)	0.56(1)
$ A(^{135}\text{Ba}) $	2.5	x	x
$ A(^{137}\text{Ba}) $	2.8	x	x
$ A(^{87}\text{Sr}) $	1.5	x	x
K ⁺ -O ⁻			
g	2.1013(3)	2.0093(3)	1.9993(3)
Pt ^{x+} -O ⁻			
g	2.0742(3)	2.0275(3)	2.0051(3)
$ A(^{195}\text{Pt}) $	0.7 (1)	0.9 (1)	0.7 (1)
$ A(^{135}\text{Ba}) $	2.31 (5)	2.52 (5)	2.34 (5)
$ A(^{137}\text{Ba}) $	2.58 (5)	2.87 (5)	2.62 (5)
$ A(^{87}\text{Sr}) $	1.6 (1)	1.6 (1)	x
I-O ⁻			
g	2.0640(3)	2.0280(3)	2.0075(3)
II-O ⁻		[1 $\bar{1}$ 0] + τ	[110] + τ
$\tau = 18^\circ$ *			
g	2.0708(3)	2.0275(3)	2.0080(3)
III-O ⁻		[1 $\bar{1}$ 0] + τ	[110] + τ
$\tau = 18^\circ$ *			
g	2.0640(3)	2.0270(3)	2.0070(3)

Also interaction with Sr nuclei (⁸⁷Sr, $I = 9/2$, 7.0%), present as a background impurity, is identified. The stick diagrams interpreting the hyperfine structures, using the values in Table I, are indicated in the lower part of Fig. 3. It is seen that each of the four Na lines is accompanied by a set of further structures. The sum of these sticks, convoluted with the widths of the Na lines, leads to a rather detailed coincidence between observed and measured spectra.

After K doping (1000 mol ppm K₂O in the melt) new resonances with topologically identical angular dependences arise after illumination; their parameters are also listed in Table I. Representative spectra of O⁻-Na⁺ and O⁻-K⁺ are compared in Fig. 4. Since the magnetic moment of K (³⁹K, $I = 3/2$, 93%) is only 0.18 times that of Na, the hyperfine splitting of K is not resolved. The additional structure beside the main K line in Fig. 4 can be attributed to further hyperfine interaction with three Ba ions next to O⁻.

Besides these fundamental defects several other ones of similar structures have been discovered. The parameters of the most prominent one among them are likewise given in Table I. A typical spectrum is shown in Fig. 5. In addition to the outer hyperfine lines, assigned as indicated, there is the strong central structure, attributed to an element with a mixture of nonmagnetic and magnetic ($I = 1/2$) isotopes, the latter with an abundance between 20% to 40%. There are two such elements in nature: ¹⁹⁵Pt ($I = 1/2$, 33.8%) and ²⁰⁷Pb ($I = 1/2$, 22.1%), the remaining isotopes having $I = 0$. It turns out that the assumption "Pt" leads to a somewhat better fit of the spectra. Pt is expected and found² to replace Ti in BaTiO₃. The ESR analysis demonstrates that O⁻ next to Pt also has a π -orbital ground state as shown in Fig. 2, i.e., the

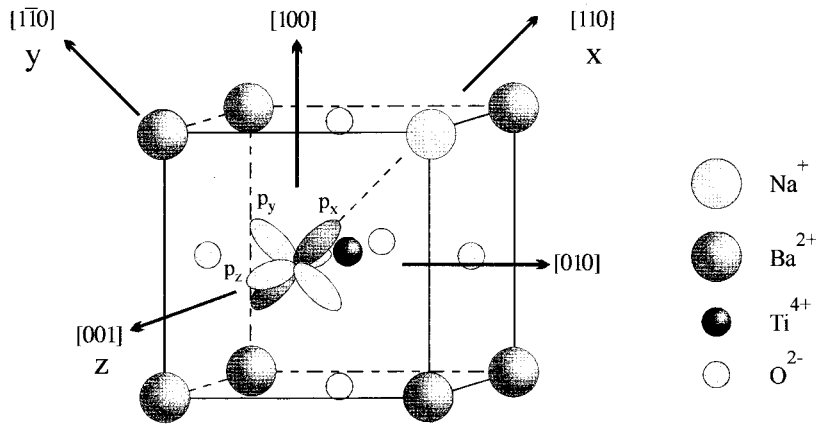


FIG. 2. Orbital model of O^{2-} next to Na_{Ba}^+ , with the designations used for further reference. The ground state, shown dark, is always assumed to be p_x .

p lobe of the ground state does not point to the acceptor defect, Pt_{Ti} . The charge state of Pt in $O^- - Pt_{Ti}$ is not yet known.

Table I also collects information on three similar further defects in $BaTiO_3$. To this group there belong two types, "II" and "III," having their g axes tilted away from the $\langle 110 \rangle$ type axes by 18° in both cases, as indicated in Table I. Except for this rotation the g tensors of these defects are similar to center "I" and to $Pt-O^-$. The concentration of the tilted centers increases under reduction. It should be remarked that none of the alkali centers (Na^+ and K^+) has a tilted counterpart.

In this context we add that spectra now attributed to $Na^+ - O^-$ have also been reported by Schwartz *et al.*¹⁰ Hyperfine interaction was not resolved and resonances were not

detected for some essential directions of the magnetic field; therefore the underlying center was erroneously claimed to be axially symmetric.

B. Analysis of ESR data

We shall show that the observed Zeeman and hyperfine interactions of $Na^+ - O^-$ and $K^+ - O^-$ can be understood on the basis of the orbital level scheme expected for O^- ($2p^5, L=1$), situated on the axis between two Ti^{4+} ions in $BaTiO_3$ and weakly perturbed by a neighboring Na_{Ba}^+ acceptor core; see Fig. 2. The symmetry of the unperturbed O^- site is D_{4h} , neglecting minor influences which might be caused by the slight deviation of the low-temperature rhombohedral phase of $BaTiO_3$ from a cubic structure.

The crystal field Hamiltonian for this situation is

$$\mathcal{H}_{cf} = DL_z^2 + E(L_x^2 - L_y^2) + \lambda LS, \quad (1)$$

where the orthorhombic perturbation by the Na acceptor and by spin-orbit interaction is taken into account, and the axes

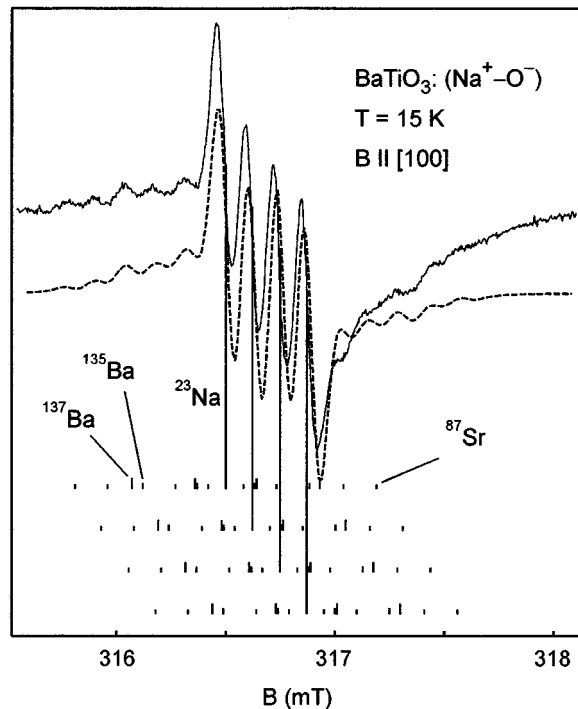


FIG. 3. Na, Ba, and Sr superhyperfine interaction of $Na^+ - O^-$ and their simulation ($\nu = 9.291$ GHz; modulation amplitude: $24 \mu T$; microwave power: 5.1 mW; light intensity: 30 W/m²; light energy: 2.88 eV).

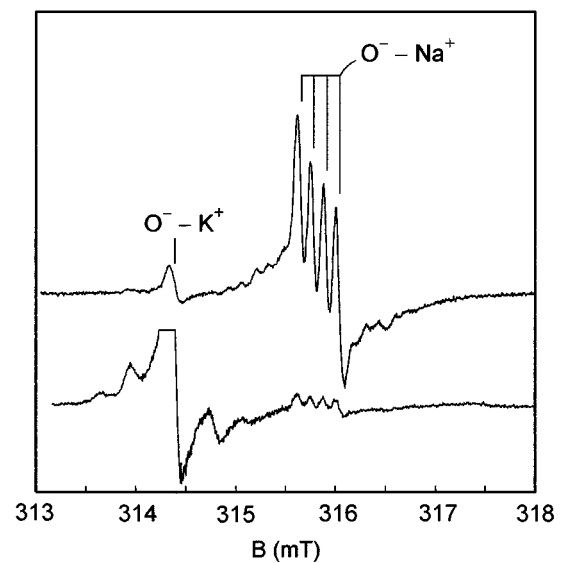


FIG. 4. Comparison of the Na^+ and K^+ resonances obtained with an as grown and with a Na-depleted, K-enriched sample ($\nu = 9.265$ GHz, modulation amplitude: $24 \mu T$; microwave power: 5.1 mW; $T = 9$ K; $B || [100]$; light intensity: 30 W/m²; light energy: 2.88 eV).

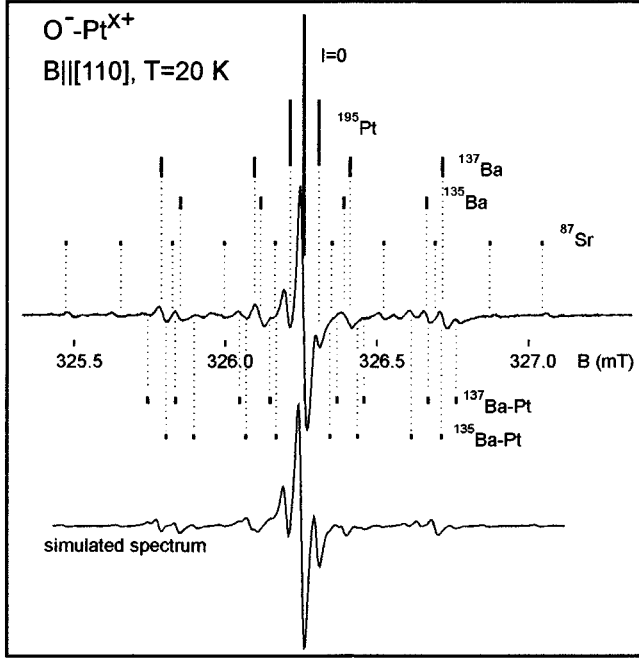


FIG. 5. Superhyperfine structure of O⁻ assumed to be associated with Pt_{Ti}^{X+}. The assignments of the components are indicated. A simulation of the experimental spectrum is given ($\nu=9.258$ GHz; modulation amplitude: 24 μ T; microwave power: 5.1 mW; light intensity: 30 W/m²; light energy: 2.88 eV).

are oriented as given in Fig. 2. An orbital singlet, p_z , is highest in the hole picture, separated by D from a doublet, which is split by $2(E^2 + \lambda^2/4)^{1/2}$. In the case of vanishing spin-orbit coupling the doublet orbitals are p_x and p_y . In Fig. 2, p_x has been assumed to be the ground state.

1. g tensors

We can make use of the similarity of the ESR features of the present centers to those of the O₂⁻ molecule in the alkali halides.¹¹ In the latter case a hole moves in an orbitally two-fold degenerate Π_g orbital of the strongly axial molecule. The two components of Π_g correspond to the p_x and p_y states in the present O⁻ centers. Since the O₂⁻ axis extends along a $\langle 110 \rangle$ direction in an alkali halide crystal, the symmetry of the molecule is orthorhombic and the degeneracy of the Π_g orbitals is lifted.

If the spin-orbit mixture of the two lowest levels is exactly taken into account and the admixture of the highest one up to second order, one arrives at

$$\begin{aligned} g_{110} &= g_e \cos 2\alpha - g_l(\lambda/D)(\cos 2\alpha + 1 - \sin 2\alpha) - C, \\ g_{\bar{1}10} &= g_e \cos 2\alpha - g_l(\lambda/D)(\cos 2\alpha - 1 + \sin 2\alpha) + C, \\ g_{001} &= g_e + 2g_l \sin 2\alpha - C, \end{aligned} \quad (2)$$

with $\tan(2\alpha) = \lambda/2E$ and $C = g_e(\lambda^2/4D^2)(1 - \sin 2\alpha)$.

These expressions are identical to those of Zeller and Känzig,¹¹ except that here the terms C , being of second order in λ/D , are included. It turns out, however, that the latter are always smaller than 5×10^{-5} , using $\lambda_{O^-} = -150$ cm⁻¹ (see, for example, Ref. 12) and the D values derived from

TABLE II. Crystal field parameters D and E (in cm⁻¹), derived from g_{001} and $g_{\bar{1}10}$ (Table I), and comparison of experimental and predicted values g_{110} .

	D	E	$g_{110}(\text{exp})$	$g_{110}(\text{pre})$
Na ⁺ -O ⁻	39000	1600	1.9998	2.0003
K ⁺ -O ⁻	30500	1500	1.9993	1.9999
Pt-O ⁻	11000	2100	2.0051	2.0013
I-O ⁻	11100	2400	2.0075	2.0016

the first order terms; see Table II. We assume that $g_l = 1$, since orbital reduction by admixture of orbitals of neighboring ions can be neglected for the two lowest states (see Fig. 2), which give the decisive contributions to Eq. (2).

Using these expressions, the E and D values in Table II have been determined from g_{001} and $g_{\bar{1}10}$, as referred to Fig. 2. The g_{110} values predicted on this basis coincide with the experimental ones for O⁻-Na⁺ and O⁻-K⁺, Table II. For the remaining centers the experimental g_{110} values are always somewhat larger than predicted. Reasons for these slight discrepancies will be discussed below in Sec. IV.

2. Na hyperfine interaction

Table I contains the parameters of the Na-hyperfine interaction. We know from the analysis of g that the ground state p orbital points along the x direction; see Fig. 2. Since the symmetry of the center is orthorhombic, the hyperfine tensor A has the same principal axes as g . All components of the hyperfine tensor have the same sign; only under this assumption can the hyperfine structure of the spectra be reproduced by a theoretical simulation.¹³ Large differences to the experiment are found especially for directions of B deviating from the principal directions of A , if different signs for the components of A are assumed.

Decomposing A into its isotropic (a), axial (b), and orthorhombic (e), parts

$$A_{110} = a + 2b,$$

$$A_{\bar{1}10} = a - b - e,$$

$$A_{001} = a - b + e,$$

one arrives at $|a| = 1.02(1)$, $|b| = 0.23(1)$, and $|e| = 0.04(1) \times 10^{-4}$ cm⁻¹, the axis pointing along $[110]$; see Fig. 2. Since $|A_{110}| < |A_{\bar{1}10}|$, $|A_{001}|$, $\text{sign}(a) \neq \text{sign}(b)$. Because the p_x ground state lies in the region, where the axial hyperfine interaction, $b \propto \langle p_x | (3 \cos^2 \vartheta - 1) / R^3 | p_x \rangle$ is positive (ϑ : polar angle with respect to the Na⁺-O⁻ direction), the isotropic hyperfine interaction, a , must be negative. Since in a multielectron system all isotropic hyperfine interactions with electron spins are proportional to $(\sum_{i\uparrow} |\psi_i^\uparrow(\mathbf{r})|^2 - \sum_{j\downarrow} |\psi_j^\downarrow(\mathbf{r})|^2)$, where \mathbf{r} means the site of the nucleus whose hyperfine coupling is probed, where \uparrow is the spin direction of the main unpaired electron and where the sums are over all orbitals having finite amplitude at \mathbf{r} , $a < 0$ means that the spin density at the Na nucleus is opposite to that of O⁻ p_x . This is astonishing, since p_x has finite overlap with Na⁺. The situation differs from that where the interacting nucleus lies on a nodal plane of the ground state

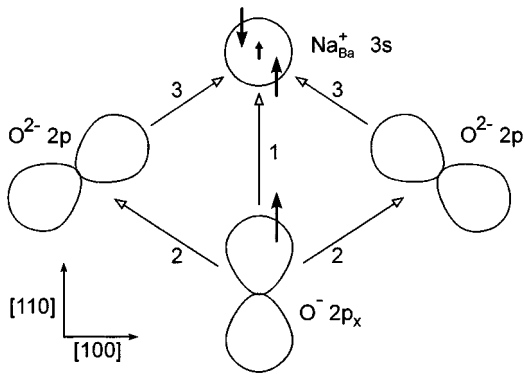


FIG. 6. Orbital scheme used to illustrate direct and indirect O^- - Na^+ overlap. The ground state orbital $2p_x$ transfers \uparrow to the Na nucleus by direct overlap, path 1. The shown $O^{2-} 2p$ orbitals represent two out of a total of four such ions pairwise lying above and below the $(1\bar{1}0)$ plan containing (O^-Na^+) . The indirect overlap of $O^- 2p_x$ along paths 2 and 3 decreases the \uparrow density at the Na nucleus.¹⁷ Exchange polarization of the \uparrow and \downarrow Na s orbitals then leads to a \downarrow majority at the Na nucleus.

orbital, populated by the main unpaired electron. It is well known that in this case, exchange core polarization of paired electrons in innershell orbitals having nonzero density at the relevant nucleus can lead to $a < 0$.^{14,15}

In the present geometry we encounter the fact that the strong overlap of the $O^- p_x$ orbital with the Na nucleus would produce a large positive a . For a similar situation, O^-Li^+ in MgO, CaO, SrO,¹⁶ we have demonstrated earlier¹⁷ that the density of the main unpaired electron at the Li nucleus, corresponding to the Na nucleus in the present situation, can be strongly reduced by destructive interference between the electron amplitudes along path 1 in Fig. 6, describing the direct overlap of the p_x orbital with the Na s shells, and along paths 2 and 3, taking account of indirect overlap. In this way a situation is produced similar to the case of a nucleus lying on a nodal plane. Exchange core polarization of the Na s orbitals can then lead to $a < 0$. This has been demonstrated in the case treated earlier,¹⁷ and not only the sign, $a < 0$, but also the amount of a has been predicted in almost quantitative agreement with observation.

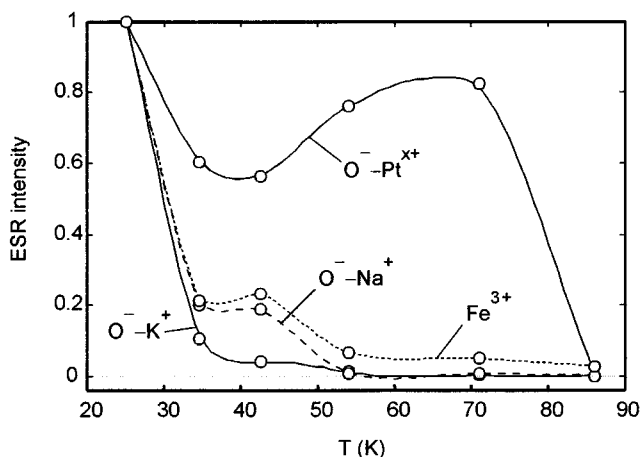


FIG. 7. Temperature dependence of the ESR intensity of the O^- and Fe^{3+} centers, determined by isochronal anneal, after pumping by near bandgap illumination at 25 K.

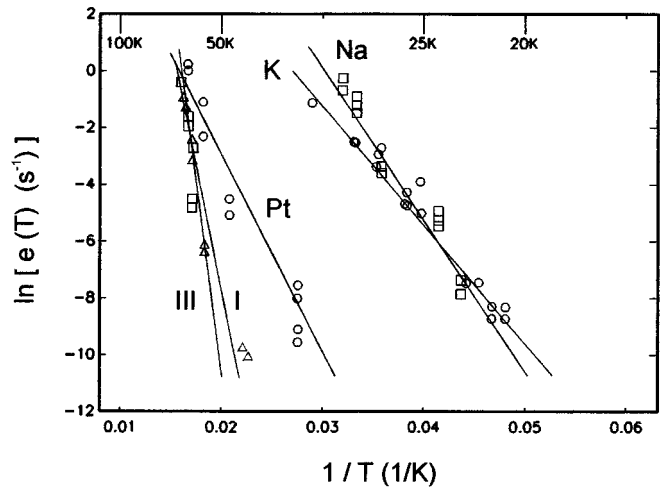


FIG. 8. Decay rates $e(T)$ of nonequilibrium hole populations, introduced by near bandgap illumination at low temperatures for various O^- centers. The designations are related to those given in Table I. A corresponding plot including a correction by T^2 (see text) is not shown.

The size of the axial hyperfine interaction parameter, b , contains information on the distance, R , between nucleus and O^- site. Considering, as a boundary case, the situation that the O^- orbital shrinks to a point, we have $b(R) = (\mu_0/4\pi)g_e\mu_B g_n \mu_K \langle R^{-3} \rangle$. Comparison with the experimental b yields $R = 0.312$ pm, $\sim 10\%$ longer than the distance expected for an undistorted lattice, 0.285 pm. The elongation of the O^-Na^+ distance can be understood as follows: The O^- ion is attracted more strongly by its twofold positive neighbors, Ba^{2+} (or Sr^{2+}) than by the onefold positive Na^+ . It must be added that corrections for the finite size of the $O^- p_x$ orbitals will not change this result decisively.

C. Thermal stability of the neutral state of the alkali acceptors

Using the method of isochronal anneal, i.e., heating to a given temperature, holding this for 2 minutes and fast cool-

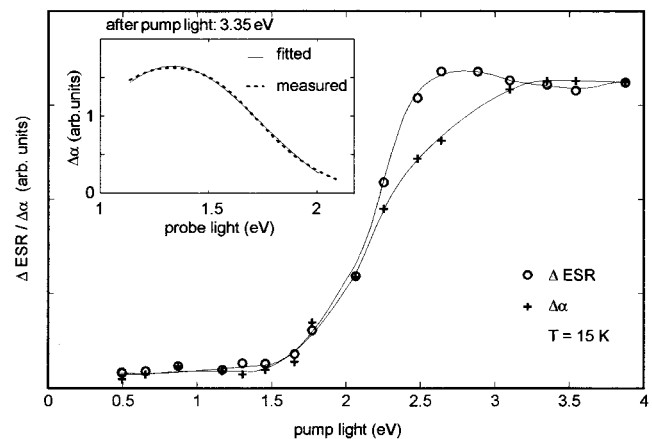


FIG. 9. Parallel rise of O^-Na^+ ESR and optical absorption, simultaneously measured at 15 K under illuminations with light of increasing energies, starting at 0.5 eV. The deviation between both curves, being guides to the eye, near 2.3 eV is caused by an overlapping band decreasing in intensity under illumination with light of this energy. The inset shows the O^- band along with its theoretical reproduction.

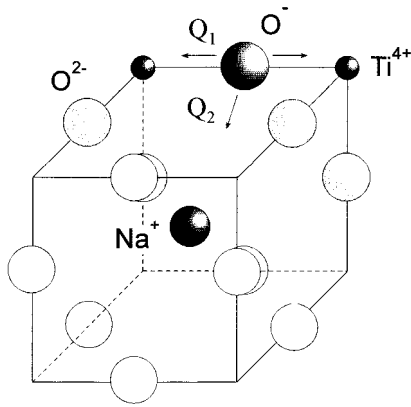


FIG. 10. The twelve oxygen ions surrounding Na_{Ba}^+ one of the O^{2-} has been transformed to O^- (dark) by capturing a hole. Light-induced polaronic hole transfer can take place to the nearest O^{2-} neighbors (grey). The tetragonal distortion, Q_1 , can be assumed to lead to a stronger decrease of energy than Q_2 ; the latter affects only the rather long and therefore weak $\text{Na}^+-\text{O}^{2-}$ bond.

ing to 25 K, where ESR is measured, the signal heights given in Fig. 7 were obtained. Holes captured near the alkali acceptors are thermally ionized already at 50 K; the Pt- O^- acceptor is more stable, losing its hole only near 85 K. Also the temperature dependence of the Fe^{3+} signal, present as a further impurity in the crystal, is shown. A close correlation to the intensity of Na^+-O^- is seen. Apparently the holes thermally ionized from Na^+-O^- are captured at Fe^{3+} , forming Fe^{4+} . This may be caused by a spatial proximity between Na^+ and Fe^{3+} . It is not known why such a correlation is not observed for K^+-O^- . Also the centers I, II, and III in Table I have a high thermal stability, comparable with that of O^- -Pt. This might indicate that these defects likewise contain acceptor ions on the Ti site. In this context it should be remarked that also $\text{Al}^{3+}-\text{O}^-$ is thermally ionized near 100 K. This ion certainly replaces Ti; its structure, however, is somewhat different, the hole being shared by two O^- ions.² Because of the shorter distance between O^- and an acceptor ion on a Ti site, such defects are expected to be more stable than O^- - Na_{Ba}^+ and similar centers.

D. Energy levels

The low temperatures at which the acceptors are thermally ionized (Fig. 7) suggest that their energy levels are close to the valence-band edge. They were determined by monitoring their hole emission rates, $e(T)$, as depending on temperature. This was possible since it was noticed that during high intensity illumination of the crystals the hole population of the acceptors was higher than in the equilibrium situation, attained at long times after illumination. Apparently these acceptors have rather large capture cross sections. The rates of the return of the excess population to equilibrium, $e(T)$, are plotted in Fig. 8. Exponential decays of $e(T)$ are observed. This is predicted by the following arguments. Detailed balance requires¹⁸ that

$$e(T) = \gamma c(T) \exp(-E_b/kT), \quad (3)$$

where γ is the ratio of the degeneracies of the valence-band edge and the acceptor, and $c(T)$ represents the capture rate.

TABLE III. Binding energies E_b , in meV, of holes at shallow acceptors in BaTiO_3 .

Acceptor	E_b/meV	E_b/meV (incl. T^2 corr.)
K^+	36 (4)	32 (4)
Na^+	46 (4)	41 (4)
Pt^{x+}	60 (5)	53 (5)
I	150 (30)	150 (30)
II	230 (30)	230 (30)

The right-hand side of Eq. (3) is dominated by the exponential, since the product $\gamma c(T)$ can be estimated to be at most proportional to T^2 : In simple cases the valence-band effective density of states is $\propto T^{3/2}$. The root mean square velocity with which the valence-band holes can be assumed to arrive at the acceptor site, having a temperature independent capture cross section, scales as $T^{1/2}$. Because it is uncertain whether these estimates are applicable also for BaTiO_3 , where strong hole phonon coupling is expected, we have evaluated the slopes in Fig. 8 by alternatively including and neglecting the T^2 correction; see Table III. The depths of the Na^+ and K^+ acceptors, ~ 45 meV and ~ 34 meV, do not depend significantly on this extra factor. Both levels are very close to the valence-band edge. Shell model calculations¹⁹ predict for the K^+ acceptor in BaTiO_3 a level energy of 120 meV, for Na^+ 60 meV.

E. Optical absorption

Under the illuminations which create the O^- ESR also a strong optical-absorption band with maximum near 1.3 eV appears; see inset in Fig. 9. Its intensity is correlated to that of the Na^+-O^- ESR in Fig. 9.

The features of the absorption band—large width, high intensity, peak in the visible or near infrared, correlation with O^- ESR—are characteristic for light-induced hole transfer between O^{2-} ions equivalent with respect to the acceptor core, Na^+ in the present case. In the past this model^{20,21,18} has successfully explained O^- -related absorptions in many materials [e.g., $\text{MgO}:\text{V}^-$ and similar defects,²¹ $\text{SiO}_2:\text{Al}^{3+}$ (smoky quartz),²² light-induced absorption in YAlO_3 ,⁴ Zn vacancy in ZnSe^{23}].

The hole can be self-trapped at each of the equivalent O^{2-} sites, and optical transfer to a neighboring site then occurs under Franck-Condon conditions. Therefore the energy of the band maximum is identical to the Franck-Condon shift, initial and final ground state energies being identical. Because of this fact there is also a correlation between band position and width: No phonon-broadened absorption band can be wider relative to its peak position. These features are characteristic for small polaron optical absorption.

Since the intensity of the optical transfer transition depends on the square of the energy overlap integral,²⁰ J , which is a function exponentially decreasing with distance, only the nearest neighbors of an initial O^{2-} ion are eligible as final sites. Among these there are the four O^{2-} ions indicated in Fig. 10, which are characterized by their equivalence with respect to Na^+ . Since the (O^- - Ti^{4+}) distance is shorter than (O^- - Na^+), the former bond can be assumed to be more de-

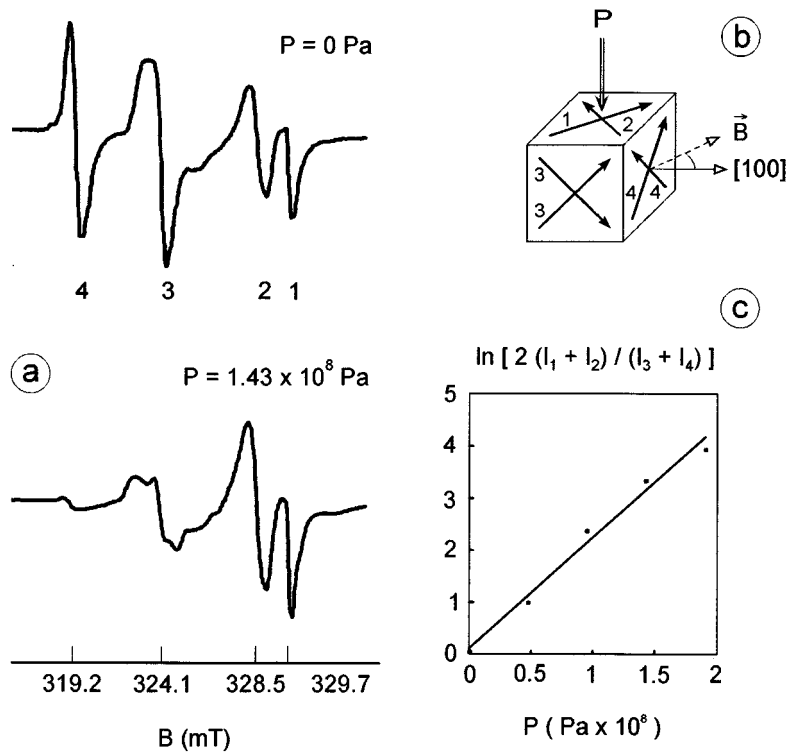


FIG. 11. Change of O^- ESR under (100) uniaxial stress (a), \vec{B} being directed as indicated in Fig. 1. (b) Relative orientations of the O^- ground state orbitals, indicated by arrows, and the stress direction. (c) Relation between relative O^- intensities and stress.

cisively influenced by capture of a hole at O^- . Therefore the self-trapping energy will be mainly determined by the axially symmetric distortion Q_1 along the (O^- - Ti^{4+}) direction. For this situation it has been demonstrated earlier,²¹ that the maximum of the optical-absorption band, resulting from the light-induced polaronic hole transfer between both sites, is at $2E_{JT}$, where E_{JT} is the decrease in energy by coupling the hole to the axial (O^- - Ti^{4+}) distortion Q_1 . It can be shown that the absorption band would be peaked at E'_{JT} , if the (Na^+ - O^-) distortion, Q_2 , was decisive, E'_{JT} being the corresponding stabilization energy. The shape of the absorption band is given by $\alpha \propto \exp[-w(E-2E_{JT})^2]$ with $w^{-1} = (4E_{JT}\hbar\omega_0)$, where $\hbar\omega_0$ is the energy of the interacting lattice vibration. It is seen in the inset of Fig. 9 that the band is well reproduced with $E_{JT} = 0.65$ eV and $\hbar\omega_0 = 0.12$ eV. The latter value is of the order of magnitude of the highest lattice vibration energies in $BaTiO_3$. E_{JT} is comparable to the values found²¹ for $MgO:V^-$ (0.97 eV) and $MgO:Na^+$ (0.67 eV). In contrast to the present situation, where the hole is in a π -orbital, in these cases it is localized in a σ bond, more strongly affecting the bond strength.

Figure 9 compares the changes of the intensity of the O^- band with those of the Na^+ - O^- ESR under illumination with a series of increasing light energies. These measurements were made simultaneously, using the setup described in Sec. II. It is seen that both phenomena are correlated to each other, supporting the assignment of the absorption band at 1.3 eV to Na^+ - O^- . The slight discrepancy between both curves in Fig. 9 near 2.3 eV is caused by the decrease of a strong and wide band, peaked at 2.3 eV, overlapping with the O^- band. This absorption at 2.3 eV is connected with the decrease of the ESR of Rh^{4+} . The creation of the holes leading to Na^+ - O^- can be attributed in this crystal to the

excitation of valence band electrons to the $Rh^{4+/3+}$ level.²⁴ In some specimens the corresponding hole photoionization of Fe^{4+} is dominant.

F. Reorientation of the Na^+ - O^- axes under uniaxial stress

Upon application of uniaxial stress at 4.2 K along a pseudocubic $[001]$ axis, with the magnetic field perpendicular to the stress direction, relative intensity changes of the Na^+ - O^- hole ESR lines are observed; see Fig. 11. The lines do not shift or become wider under stress. The experimental results can be explained by assuming that the sixfold orientational degeneracy of the Na^+ - O^- axes is partly lifted, according to Fig. 11(b), into a twofold degenerate set of lower energy and a fourfold set with higher energy levels. As expected, sites with their p_x orbitals perpendicular to the stress direction are favored. This stress dependence is analogous to that found for the Fe^{2+} - O^- hole center in $SrTiO_3$.⁵ In Fig. 11(c) $\ln[2(I_1 + I_2)/(I_3 + I_4)]$ is plotted as a function of the $[001]$ stress, where the intensities have been labeled according to Fig. 11(a). In making these measurements the Na hyperfine structure was wiped out by using overmodulation. For stresses higher than 2×10^8 Pa a deviation from the linear dependence is found. Also small hysteresis effects, due to residual strains, were observable after applying stress.

The stress-split levels are populated according to Boltzmann's distribution. Their energy difference is described by means of an elastic dipole.²⁵ The dipole energy is²⁶ $\Delta U = V_0 \lambda \mathbf{p} \equiv \boldsymbol{\beta} \mathbf{p}$, where $\boldsymbol{\beta}$ is the linear stress coupling tensor (with the dimension of a volume) and \mathbf{p} is the stress tensor. The anisotropic part of the λ tensor, λ' , has zero trace.²⁷ For a uniaxial stress along the $[001]$ direction, the differential stress coupling coefficient $\beta_{[001]}$ of an orthorhombic defect is given by²⁷ $\beta_{[001]} = V_0 [\frac{1}{2}(\lambda'_1 + \lambda'_2) - \lambda'_3]$, where λ'_1 , λ'_2 , and

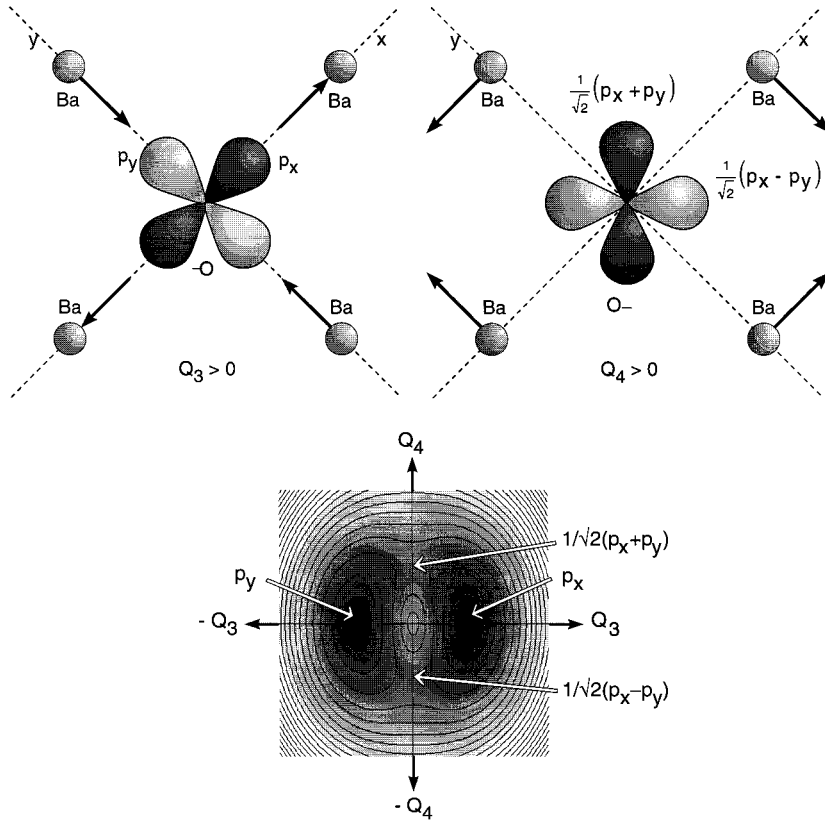


FIG. 12. (a) Asymmetric vibration modes coupling with the orbitally degenerate p_x , p_y orbitals. (b) Lower energy surface (for $E_1 < 0$) resulting from the coupling described in the text. Parameters used: $v_3 = 1$, $v_4 = 0.5$, $K_3 = 2$, $K_4 = 1$; Q_3 and Q_4 vary between ± 1.2 .

λ'_3 are the principal values of the λ' tensor. At thermal equilibrium the ESR line intensity ratio becomes $2(I_1 + I_2)/(I_3 + I_4) = \exp(\beta_{[001]}p/kT)$. From the slope of the least square fit line we find $\beta_{[001]} = 1.23 \times 10^{-30} \text{ m}^3$ at 4.2 K. This value is of the same order as that found for the $\text{Fe}^{2+} - \text{O}^-$ center in SrTiO_3 ($\beta_{[001]} = 3.48 \times 10^{-30} \text{ m}^3$ at 30 K).⁵

IV. DISCUSSION

The detailed information on the alkali- O^- centers, which is available now, invites their comparison with other O^- hole centers in oxide perovskites and in related compounds, such as the cuprate superconductors. Also in these materials the holes introduced into the CuO_2 planes by doping with acceptors situated outside of these planes, have their highest density at the O^{2-} sites, forming O^- . However, because of the high $\text{Cu}^{2+} - \text{O}^-$ covalency, holes are found in σ -type orbitals, connecting Cu^{2+} and O^- , whereas in the O^- centers in the perovskites the hole is in π -type orbitals, avoiding the neighboring Ti^{4+} sites. In stabilizing this orbital the attraction between the alkali ion on the Ba site and the O^- hole does not seem to be decisive. In fact, there are also acceptors on the Ti site, in principle attracting the hole, for which the ground state is still a π orbital. This has been shown previously, e.g., for Al^{3+} and Mg^{2+} (Ref. 8) as well as Fe^{2+} (Ref. 5) in SrTiO_3 . Also the centers attributed here to $\text{Pt} - \text{O}^-$, and to I, II, and III (Table III), although not yet definitely identified, can be assigned to acceptors on Ti sites, as will be discussed shortly. They also have π ground states. Apparently this orbital is mainly stabilized by the charge of Ti^{4+} , being at least one of the O^- neighbors, and by its lacking hole covalency with Ti^{4+} . In this context it should be remarked that a recent

embedded cluster calculation of Fe^{4+} in BaTiO_3 (Ref. 28) indicates that the ground state of this system rather is $\text{Fe}_{\text{Ti}}^{3+} + \text{O}^-$, where the O^- hole is in a π orbital.

As expected, the π orbital, however, is somewhat less favorable energetically for acceptors on the Ti site. This is seen from the D values of these defects in Table III, which are lower than those of the alkali acceptors replacing Ba. A further distinguishing feature of the acceptors on the Ti site is the sizeable discrepancy between predicted and measured g_{110} shifts (Table II). For these centers there is no symmetry breaking charge in the plane of the π -orbitals, and p_x and p_y will be essentially degenerate. These levels are then expected to be split apart by a Jahn-Teller effect (see Appendix). If this is dynamic, there will be strong vibronic deviations of the ground state orbital from the $[110]$ direction. Because of the resulting finite root mean square excursions of the p_x lobe from this direction, there will be a sizeable g shift measured for \mathbf{B} along $[110]$. According to the evaluation given in the Appendix, vibronic excursion angles of up to 20° are likely.

The comparison of the several O^- centers in the oxide perovskites demonstrates the great flexibility of the corresponding structures. The holes can be in π -type orbitals, as reported here. They can be shared by two such orbitals, forming an O_2^{3-} bond between two O^- ions neighboring each other along $[110]$ directions, as for $\text{BaTiO}_3:\text{Al}_{\text{Ti}}^{3+}$.² Such a bond can also accommodate two holes, forming a hole bipolaron.²⁹

The Ba vacancy has often been invoked as an intrinsic acceptor in BaTiO_3 . The present investigation allows us to predict the ESR signature of the Ba vacancy. This defect results from picking out the Na ion from the center shown in

Fig. 2. The angular dependence of the corresponding ESR spectra should thus be similar to those of the alkali defects, with g values closer to g_e . No such spectra have been identified. O^- centers in $SrTiO_3$ have lower maximal g shifts than those in $BaTiO_3$. This can possibly be attributed to the lower ionic radius of Sr^{2+} as compared to Ba^{2+} . Stabilizing relaxations after hole capture can thus be stronger in $SrTiO_3$, leading to larger energy splittings and thus lower g shifts.

Finally, we want to point out that one of the most important features of the alkali centers in $BaTiO_3$ is their low acceptor level. Doping with such acceptors should allow one to lower the Fermi level to a position close to the valence-band edge. It should be noted that in spite of their levels lying very near to the valence band the alkali acceptors can be treated in the localized hole picture and not with an effective mass model. This, of course, is caused by the strong hole-lattice coupling, favoring localization.

ACKNOWLEDGMENTS

We thank Dr. H. Hesse and C. Kuper for kindly supplying the crystals used in this study. The work reported here was partly supported by DFG, Sonderforschungsbereich 225.

APPENDIX: JAHN-TELLER EFFECT OF THE $O^- \pi$ ORBITALS

The O^{2-} site in ideal perovskites is axially symmetric, local group D_{4h} . The hole ground state is twofold degenerate, if spin-orbit splitting is neglected. This is the basis for a simple Jahn-Teller situation. A structurally equivalent case has been treated by Estle³⁰ in a lecture introducing to the Jahn-Teller effect. Among the vibrational modes of the planar “five-ion” molecule, O^- surrounded by four Ba^{2+} ions [Fig. 12 (a)], there are two low symmetry oscillations which can couple³¹ to the twofold degenerate orbital ground state $\Gamma_5^-(D_{4h})$. These vibrations have Γ_3^+ and Γ_4^+ symmetry, respectively. They are visualized in Fig. 12 (a). Quantifying the heuristic arguments used by Estle³⁰ we arrive at the JT Hamiltonian:

$$\mathcal{H}_{JT} = v_3 \mathcal{E}_3 Q_3 + v_4 \mathcal{E}_4 Q_4 + \frac{1}{2} K_3 Q_3^2 + \frac{1}{2} K_4 Q_4^2. \quad (A1)$$

Operating on the p_x, p_y base (Fig. 2), the electronic operators \mathcal{E}_3 and \mathcal{E}_4 have the structure

$$\mathcal{E}_3 = \begin{pmatrix} 1 & 0 \\ 0 & -1 \end{pmatrix}, \quad \mathcal{E}_4 = \begin{pmatrix} 0 & 1 \\ 1 & 0 \end{pmatrix}. \quad (A2)$$

The eigenstates of \mathcal{E}_3 are p_x and p_y , respectively; those of \mathcal{E}_4 , $(p_x \pm p_y)/\sqrt{2}$. The eigenvalues of \mathcal{H}_{JT} are

$$E_{1,2} = \pm (v_3^2 Q_3^2 + v_4^2 Q_4^2)^{1/2} + \frac{1}{2} K_3 Q_3^2 + \frac{1}{2} K_4 Q_4^2 \quad (A3)$$

and its eigenvectors

$$\Psi_g = p_x \cos \varphi + p_y \sin \varphi, \quad (A4)$$

with $\tan(2\varphi) = (v_4 Q_4)/(v_3 Q_3)$. The energy surface described by Eq. (7) is demonstrated for $E_1 < 0$ in Fig. 12(b). The minima along the Q_3 direction, stabilizing either p_x or p_y , cause the orthorhombic splitting, parameter E in Eq. (1). For O^- in $BaTiO_3$ the JT minima are expected to be rather flat, as indicated in Fig. 12 (b), because the Ba^{2+} ions, limiting the angular excursions of the p lobes are rather distant from O^- . Outside of the Q_3 axis the eigenstates are mixtures of p_x and p_y . This observation will be used to explain the observed g values for B along the x axis. We think that the deviation between predicted and observed g_{110} values in Table II is caused by the vibronic nature of the ground state Eq. (8), allowing admixtures between p_x and p_y . In an analogous way g shifts resulting from a vibronic mixture between the $(3z^2 - r^2)$ and $(x^2 - y^2)$ orbitals of, e.g., Cu^{2+} in an octahedral crystal field have been derived by O'Brien.³²

For the vibronic ground state Ψ_g the expectation value of the Zeeman operator $\mathcal{H}_z = \mu_B \mathbf{B} g \mathbf{S}$, is given by

$$\langle \Psi_g | \mathcal{H}_z | \Psi_g \rangle = \langle \cos \varphi p_x + \sin \varphi p_y | \mathcal{H}_z | \cos \varphi p_x + \sin \varphi p_y \rangle.$$

Since the vibration of the lattice surrounding the O^- ion, causing the finite angular excursions, is fast compared to the Larmor frequency, the time average of $\langle \mathcal{H}_z \rangle$ is observed:

$$\overline{\langle \mathcal{H}_z \rangle} = \cos^2 \varphi(t) \langle p_x | \mathcal{H}_z | p_x \rangle + \sin^2 \varphi(t) \langle p_y | \mathcal{H}_z | p_y \rangle.$$

The mixed term, $\overline{\cos \varphi(t) \sin \varphi(t)}$, is zero, $\cos \varphi(t)$ and $\sin \varphi(t)$ being even and odd functions of the angle $\varphi(t)$. The latter can be assumed to vary sinusoidally around zero, thus being an uneven function of time.

In order to arrive at an estimate of $\sin^2 \varphi(t)$, $\langle p_x | \mathcal{H}_z | p_y \rangle$ and $\langle p_y | \mathcal{H}_z | p_y \rangle$ must be known. The former can be identified with $g_{110} \mu_B B_{110}$, where g_{110} is the calculated value for g_{110} in Table II. An estimate for $\langle p_y | \mathcal{H}_z(B_{110}) | p_y \rangle$ can be obtained, if it is considered that this is—by symmetry (see Fig. 2)—roughly equivalent to $\langle p_x | \mathcal{H}_z(B_{110}) | p_x \rangle$. We thus have $\Delta g_{110, \text{exp}} \approx \cos^2 \varphi(t) \Delta g_{110, \text{calc}} + \sin^2 \varphi(t) \Delta g_{\bar{1}\bar{1}0}$. Here it is considered that the vibronic correction to $\Delta g_{\bar{1}\bar{1}0}$ will be small compared to $\Delta g_{\bar{1}\bar{1}0}$ (Table I), whereas it is essentially the only contribution to Δg_{110} .

Using $\cos^2 \varphi(t) = 1 - \sin^2 \varphi(t)$ we obtain

$$\Delta g_{110, \text{exp}} \approx \Delta g_{110, \text{calc}} + (\Delta g_{\bar{1}\bar{1}0} - \Delta g_{110, \text{calc}}) \sin^2 \varphi(t)$$

or

$$\frac{\Delta g_{110, \text{exp}} - \Delta g_{110, \text{calc}}}{\Delta g_{\bar{1}\bar{1}0} - \Delta g_{110, \text{calc}}} \approx \sin^2 \varphi(t).$$

The experimentally determined difference $\Delta g_{110, \text{exp}} - \Delta g_{110, \text{calc}}$ corresponds to $\sqrt{\varphi^2} \approx 20^\circ$ for O^- -Pt, which appears to be reasonable.

- ¹D. M. Smyth, *Prog. Solid State Chem.* **15**, 145 (1984).
- ²E. Possenriede, P. Jacobs, and O. F. Schirmer, *J. Phys. Condens. Matter* **4**, 4719 (1992).
- ³E. Possenriede, H. Kröse, T. Varnhorst, R. Scharfschwerdt, and O. F. Schirmer, *Ferroelectrics* **151**, 199 (1994).
- ⁴O. F. Schirmer, K. W. Blazey, W. Berlinger, and R. Diehl, *Phys. Rev. B* **11**, 4201 (1975).
- ⁵T. W. Kool and M. Glasbeek, *J. Phys. Condens. Matter* **5**, 361 (1993).
- ⁶A. Lagendijk, Ph.D. thesis, University of Amsterdam, 1974.
- ⁷E. Possenriede, O. F. Schirmer, and B. Hellermann, *Solid State Commun.* **65**, 31 (1988).
- ⁸O. F. Schirmer, W. Berlinger, and K. A. Müller, *Solid State Commun.* **18**, 1505 (1976).
- ⁹B. Henderson and J. E. Wertz, *Defects in the Alkaline Earth Oxides* (Francis & Taylor, London, 1977).
- ¹⁰R. N. Schwartz, D. A. Wechsler, and R. A. McFarlane, *Phys. Rev.* **46**, 3263 (1992).
- ¹¹H. R. Zeller and W. Känzig, *Helv. Phys. Acta* **40**, 845 (1967).
- ¹²O. F. Schirmer, *J. Phys. C* **11**, L65 (1978).
- ¹³The program package R-SPECTR by V. G. Grachev, Institute for Materials Sciences, 252180, Kiev, Ukraine, has been used.
- ¹⁴F. J. Adrian, A. N. Jette, and J.-M. Spaeth, *Phys. Rev. B* **31**, 3923 (1985).
- ¹⁵R. Gazzinelli and R. L. Mieher, *Phys. Rev. Lett.* **12**, 644 (1964).
- ¹⁶O. F. Schirmer, *J. Phys. Chem. Solids* **32**, 499 (1971).
- ¹⁷O. F. Schirmer, *J. Phys. C* **6**, 300 (1973).
- ¹⁸W. Hayes and A. M. Stoneham, *Defects and Defect Processes in Nonmetallic Solids* (John Wiley and Sons, New York, 1984), p. 215.
- ¹⁹A. Birkholz and H. Donnerberg (private communication).
- ²⁰O. F. Schirmer, P. Koidl, and H. G. Reik, *Phys. Status Solidi B* **62**, 385 (1974).
- ²¹O. F. Schirmer, *Z. Phys. B* **24**, 235 (1976).
- ²²O. F. Schirmer, *Solid State Commun.* **18**, 1349 (1976).
- ²³D. Y. Jeon, H. P. Gislason, and G. D. Watkins, *Phys. Rev. B* **48**, 7872 (1993).
- ²⁴H. Kröse, R. Scharfschwerdt, O. F. Schirmer, and H. Hesse, *Appl. Phys. B* **61**, 1 (1995).
- ²⁵A. S. Nowick and W. R. Heller, *Adv. Phys.* **12**, 251 (1963).
- ²⁶L. D. Landau and E. M. Lifshitz, *The Theory of Elasticity* (Pergamon Press, Oxford, 1975), p. 12.
- ²⁷D. Schoemaker and A. Lagendijk, *Phys. Rev. B* **15**, 115 (1977).
- ²⁸S. Többen and H. Donnerberg (private communication).
- ²⁹H. Donnerberg and A. Birkholz, *J. Phys. Condens. Matter* **7**, 327 (1995).
- ³⁰T. L. Estle, in *Optical Properties of Ions in Solids*, Vol. 8 of *NATO Advanced Study Institute, Series B: Physics*, edited by B. di Bartolo (Plenum, New York, 1974), pp. 419–448.
- ³¹G. F. Koster, J. O. Dimmock, R. G. Wheeler, and H. Statz, *Properties of the 32 Point Groups* (MIT Press, Cambridge, MA, 1963).
- ³²M. C. M. O'Brien, *Proc. R. Soc. London Ser. A* **281**, 323 (1964).